Appl. Phys. B 69, 29–33 (1999) / Digital Object Identifier (DOI) 10.1007/s003409901452

Applied Physics B
Lasers
and Optics

Dynamics of the Yb^{3+} to Er^{3+} energy transfer in $LiNbO_3$

E. Cantelar, F. Cussó

Departamento de Física de Materiales, C-IV, Universidad Autónoma de Madrid, 28049 - Madrid, Spain
(E-mail: fernando.cusso@uam.es)

Received: 15 October 1998/Revised version: 24 November 1998/Published online: 24 February 1999

Abstract. The energy transfer dynamics between Yb^{3+} and Er^{3+} ions in lithium niobate is investigated after ytterbium-pulsed excitation at 920 nm. The sensitisation of the $LiNbO_3$:Er^{3+} system with Yb^{3+} ions does not modify the lifetime of the $^4I_{13/2}$ erbium level (1.5-μm emission), whereas it induces a marked, concentration-dependent change in the lifetime of the $^2F_{5/2}$ (Yb^{3+}) and $^4S_{3/2}$ (Er^{3+}) multiplets (1060-nm and 550-nm emissions, respectively). The results are analysed by using the rate-equation formalism and cross-relaxation model for the energy transfer.

PACS: 42.70.Hj; 78.55.-m

The energy transfer from Yb^{3+} to Er^{3+} in lithium niobate ($LiNbO_3$) has been recently studied under cw excitation. An efficient energy transfer from Yb^{3+} to Er^{3+} has been found and it has been characterised using the rate-equation formalism in the steady-state approximation. In this way, under continuous illumination, the comparison of the Er^{3+} emission intensities at around 1.0 μm and 1.5 μm in samples co-doped with fixed Er^{3+} concentration and different Yb^{3+} concentrations allows the deterination of the transfer and back-transfer coefficients ($C_{25} = 2.4 \times 10^{-16}\,\mathrm{cm^3\,s^{-1}}$ and $C_{52} = 1.8 \times 10^{-16}\,\mathrm{cm^3\,s^{-1}}$) which quantify the transfer process [1].

Nevertheless, the transfer process is obviously a dynamic process, whose temporal behaviour needs also to be described in order to fully understand the underlying physics and facilitate further exploitation of the potentialities of this material in integrated optic devices [2–4].

In this work, the energy transfer dynamics between Yb^{3+} and Er^{3+} ions in lithium niobate is investigated. The temporal evolution of the different infrared and visible emissions detected in the $LiNbO_3$:Er^{3+}/Yb^{3+} system, and the dependence with the ytterbium concentration have been analysed after selective Yb^{3+}-pulsed excitation. The rate equation formalism is now applied in the time-dependent regime and their predictions contrasted with the experimental results.

The results not only show the temporal details of the Yb^{3+} to Er^{3+} energy transfer, including the concentration dependencies, but also constitute a rigorous test for the rate-equation formalism and transfer parameters previously obtained under cw conditions.

1 Experimental

Single crystals of Er^{3+} and Yb^{3+} co-doped $LiNbO_3$ have been grown by the Czochralski method with automatic diameter control by crucible weighting system. The starting materials were congruent $LiNbO_3$ and erbium and ytterbium oxides. The crystals have a fixed Er^{3+} concentration (0.5 mol. %) and five different Yb^{3+} concentrations (0.1, 0.5, 1.0, 1.5, and 2.0 mol. % in the melt).

Lifetime measurements were obtained at room temperature, under pulsed excitation around 920 nm using a MOPO. The fluorescence was analysed through an ARC monochromator model SpectraPro 500-i and then detected synchronously with a photodetector and recorded by a digital oscilloscope.

For infrared (IR) radiation (1.5 μm and 1.0 μm) a Judson InGaAs photodiode and amplifier were used. The temporal resolution of the system was typically of $\tau_{res} \approx 30\,\mu s$. For visible radiation, an EMI-9558QB photomultiplier tube was used, and the temporal resolution of the system was considerably shortened. In this spectral range it was now limited by the laser pulse width (10 ns).

Geometry for luminescence collection has been carefully designed in order to avoid radiation trapping effects in the temporal evolution of the 1.5-μm and 1.0-μm erbium and ytterbium emissions respectively [5].

2 Results and discussion

2.1 General spectroscopic properties of the $LiNbO_3$:Er^{3+}/Yb^{3+} *system*

The energy transfer between Yb^{3+} and Er^{3+} can be described with the help of the energy level diagram sketched in Fig. 1 and the processes indicated there. The energy overlap between the $^2F_{5/2}$ (Yb^{3+}) and $^4I_{11/2}$ (Er^{3+}) multiplets is

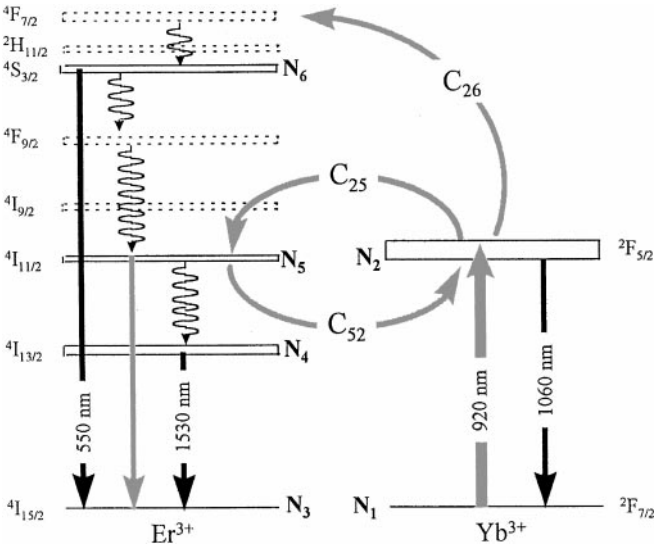

Fig. 1. Schematic energy level diagram of $LiNbO_3$:Er^{3+}/Yb^{3+} showing the multiplets involved in the energy transfer and up-conversion processes as well as the principal emissions

the basic fact that allows the efficient resonant transfer between both ions. Nevertheless, the Yb^{3+} transitions; either the absorption (associated with the $^2F_{5/2} \rightarrow {}^2F_{7/2}$ transition) or the emission (associated with the $^2F_{7/2} \rightarrow {}^2F_{5/2}$ transition), are broader than the corresponding Er^{3+} transitions. In this way it is possible to perform selective excitation of the Yb^{3+} ions (in the wavelength range 900–950 nm) and to detect the Yb^{3+} luminescence (in the range 1050–1100 nm). This possibility has been used to explore the dynamic behaviour of the Yb^{3+} to Er^{3+} energy transfer after pulsed excitation of the Yb^{3+} ions.

After the selective excitation of the $^2F_{5/2}$ (Yb^{3+}) manifold, it may relax radiatively to the $^2F_{7/2}$ ground state, producing luminescence in the range 920–1100 nm, or transfer to the $^4I_{11/2}$ level of Er^{3+} ions, according to the cross-relaxation mechanism: $^2F_{5/2} \rightarrow {}^2F_{7/2}$ (Yb^{3+}): $^4I_{15/2} \rightarrow {}^4I_{11/2}$ (Er^{3+}) and characterised by a "transfer coefficient" C_{25}.

From the $^4I_{11/2}$ erbium multiplet the excitation can be transferred back to the Yb^{3+} ("transfer coefficient" C_{52}) or relax within the Er^{3+} ions. This relaxation produces luminescence at around 1.0 μm (associated with the $^4I_{11/2} \rightarrow {}^4I_{15/2}$ transition), and at around 1.5 μm (associated with the $^4I_{13/2} \rightarrow {}^4I_{15/2}$ transition) after population of the metastable erbium level via a non-radiative connection. Whereas the 1.5-μm emission can be easily measured the 1.0-μm emission is hidden by the broader Yb^{3+} emission within similar wavelength range.

A third process, which involves the transfer of a second photon from Yb^{3+} to the $^4I_{11/2}$ Er^{3+} excited level (according to the cross-relaxation mechanism: $^2F_{5/2} \rightarrow {}^2F_{7/2}$ (Yb^{3+}): $^4I_{11/2} \rightarrow {}^4F_{7/2}$ (Er^{3+})) generates infrared to visible energy up-conversion in the erbium ions [1, 6]. In this way the erbium ions are excited to the $^4F_{7/2}$ level which relaxes non-radiatively to the $^4S_{3/2}$ level, from where (green) emission at around 550 nm is observed. This excitation mechanism is highly efficient in some materials, allowing up-conversion laser generation [7]. In $LiNbO_3$, the $^4S_{3/2}$ level has a relatively low quantum efficiency ($\eta = 0.3$) [8] and there is a relevant non-radiative relaxation back to the $^4I_{11/2}$. Let us also remember that according to the spectroscopic properties of Er^{3+} in lithium niobate [9, 10], the intermediate ($^4F_{9/2}$ and $^4I_{9/2}$) Er^{3+} levels experience a fast non-radiative decay, and their populations (and contributions to the luminescence) can be ignored.

Therefore, as summarised in Fig. 1, three luminescent emissions are observed after Yb^{3+} excitation: two infrared emissions, at $\lambda_{em} = 1.5\,\mu m$ (Er^{3+}) and $\lambda_{em} = 1.0\,\mu m$ (Er^{3+}/Yb^{3+}), plus a visible Er^{3+} emission at $\lambda_{em} = 550$ nm. These emissions can be used to study the dynamics of the energy transfer between Yb^{3+} and Er^{3+}.

2.2 Rate equations

According to the standard description of Er^{3+}/Yb^{3+} co-doped materials [11–14], the energy transfer between Yb^{3+} and Er^{3+} ions can be described by using a rate-equation formalism, which is summarised by the following rate equations:

$$\frac{dN_2}{dt} = \sigma_{Yb}\phi N_1 - (A_{21} + W_{21}^{NR})N_2 - C_{25}N_2N_3 + C_{52}N_5N_1 - C_{26}N_2N_5\,, \quad (1)$$

$$\frac{dN_4}{dt} = (A_{54} + W_{54}^{NR})N_5 + A_{64}N_6 - (A_{43} + W_{43}^{NR})N_4\,, \quad (2)$$

$$\frac{dN_5}{dt} = (A_{65} + W_{65}^{NR})N_6 + C_{25}N_2N_3 - C_{52}N_5N_1 - C_{26}N_2N_5 - (A_{54} + A_{53} + W_{54}^{NR})N_5\,, \quad (3)$$

$$\frac{dN_6}{dt} = C_{26}N_2N_5 - (A_{65} + A_{64} + A_{63} + W_{65}^{NR})N_6\,, \quad (4)$$

$$N_3 + N_4 + N_5 + N_6 = N_{Er}\,, \quad (5)$$

$$N_1 + N_2 = N_{Yb}\,, \quad (6)$$

where N_i is the population density of the ith-level, A_{ij} and W_{ij}^{NR} the radiative and non-radiative transition probabilities between the i and j states, σ_{Yb} is the Yb^{3+} absorption cross section at the pumping wavelength, ϕ is the pumping flux, and finally C_{25}, C_{52}, and C_{26} are coefficients (in units of $cm^3\,s^{-1}$) which quantify the energy transfer, the back-transfer and the up-conversion processes, respectively.

The spectroscopic parameters (transition probabilities) of Er^{3+} and Yb^{3+} in $LiNbO_3$ are reported in the literature [9, 10], and the transfer and back-transfer coefficients (C_{25} and C_{52}) have been previously determined for the system $LiNbO_3$:Er^{3+}/Yb^{3+} from cw experiments ($C_{25} = 2.4 \times 10^{-16}$ and $C_{52} = 1.8 \times 10^{-16}\,cm^3\,s^{-1}$ [1]). The remaining transfer parameter (C_{26}) can be estimated from the ratio between the electric dipole strengths of the $^4I_{11/2} \rightarrow {}^4F_{7/2}$ and $^4I_{11/2} \rightarrow {}^4F_{7/2}$ transitions [9, 10], and therefore $C_{26} \approx 2C_{25}$.

The set of (1)–(6) include in fact all the dynamic information needed to explore the temporal behaviour of the Yb^{3+} to Er^{3+} energy transfer. In the experimental conditions used in this work, the excitation is selective to the Yb^{3+} ions ($\lambda_{exc} = 920$ nm) and the pump pulse (10 ns) can be considered instantaneous as compared with the characteristic relaxation times of the luminescent transitions, as will be shown next. Therefore these conditions can be easily introduced in the rate equations and proceed to the numerical integration of (1) to

(6) to obtain the different populations (N_i) and the temporal evolution of the luminescence intensity.

2.3 Temporal evolution

2.3.1 1.5-μm *(Er^{3+}) emission.* Figure 2 shows (in a logarithmic scale) the temporal evolution of the luminescence of Er^{3+} ions ($^4I_{13/2} \rightarrow {}^4I_{15/2}$ transition), measured at 1.53 μm, after pulsed excitation of the Yb^{3+} ions for a sample co-doped with 0.5 mol. % Er^{3+} and 1.0 mol. % Yb^{3+}. As can be observed the experimental data (open circles) are in excellent agreement with the predictions from the integration of the rate equations (continuous line).

After an initial rise, the luminescence reaches a maximum ($t_{max} \approx 1$ ms) and then decays following a single exponential dependence with a time constant of 3.0 ms, independently of the Yb^{3+} concentration. This value corresponds to the lifetime observed for this transition in erbium-doped lithium niobate [5], indicating that ytterbium co-doping does not alter the lifetime of the $^4I_{13/2}$ erbium level.

As far as the initial rise time (which is also independent of the ytterbium concentration) is concerned, it has to be related to the time needed to populate the $^4I_{13/2}$ emitting level and, as can be seen in Fig. 2, it is precisely predicted by the rate-equations model. A closer inspection of the possible physical origin of this rise time shows immediately that there are two processes involved (see Fig. 1):(i) the energy transfer (and back-transfer) between Yb^{3+} to Er^{3+} and (ii) the non-radiative decay from the $^4I_{11/2}$ level to the $^4I_{13/2}$ level. This latter process, with a characteristic time given basically by the $^4I_{11/2}$ lifetime ($\tau = 220$ μs, [9]) is in fact responsible for the observed rise time, whereas the former (transfer and back-transfer) is completed in a much shorter time (tens of μs) as can be verified from the integration of (1)–(6), shown next.

2.3.2 1.0-μm *(Yb^{3+}) emission.* Figure 3 shows (also in a logarithmic scale) the experimental (open symbols) and calculated (lines) decay of the luminescence at 1060 nm, associated with the de-excitation of the Yb^{3+} ions, for all the doping concentrations studied in this work. It should be remembered that although the emission from the Yb^{3+} ions ($^2F_{5/2} \rightarrow {}^2F_{7/2}$, transition) overlaps with that of the Er^{3+} ions ($^4I_{11/2} \rightarrow {}^4I_{15/2}$ transition) in a wide wavelength range (966 nm $< \lambda_{emi} <$ 1029 nm), the Yb^{3+} emission is broader (a similar situation was already mentioned in connection with the absorption) and it is possible to select the appropriate wavelength range (1050 nm $< \lambda_{emi} <$ 1100 nm) to isolate the emission from the Yb^{3+} ions.

The lifetime of the Yb^{3+} ions in the co-doped crystals is strongly reduced from its value in Yb^{3+}-doped lithium niobate ($\tau = 580$ μs [6]). Now the lifetimes vary from 390 μs for the crystals with the higher Yb^{3+} doping level (2.0 mol. % Yb^{3+}) to 260 μs for the less concentrated samples (0.1 mol. % Yb^{3+}). This lifetime reduction (compared with Yb^{3+}-doped samples) indicates that an additional relaxation channel has been activated (that is, the energy transfer from Yb^{3+} to Er^{3+}).

The lines in Fig. 3 represent the predictions of the rate equations, calculated for the different ytterbium concentrations. It can be observed that there is an excellent accordance between the experimental data and the predictions from the model, including the concentration dependence of the Yb^{3+} lifetime. At low Yb^{3+} concentration the transfer to Er^{3+} is very efficient and the lifetime is strongly reduced; whereas increasing Yb^{3+} concentration favours the back-transfer and the observed lifetime approaches that of Yb^{3+} ions [1, 6, 15].

It should be noticed also that at shorter times, the rate equations predict a fast component (tens of μs) related to the transfer rate from Yb^{3+} to Er^{3+}, which is the dominant process initially. Unfortunately this fast component has not been experimentally accessible because it is shorter than the time response of the infrared detection system ($\tau_{res} \approx 30$ μs).

2.3.3 550-nm *(Er^{3+}) "up-conversion" emission.* Figure 4 shows the comparison between the temporal evolution of the green up-conversion luminescence of Er^{3+} ($^4S_{3/2} \rightarrow {}^4I_{15/2}$

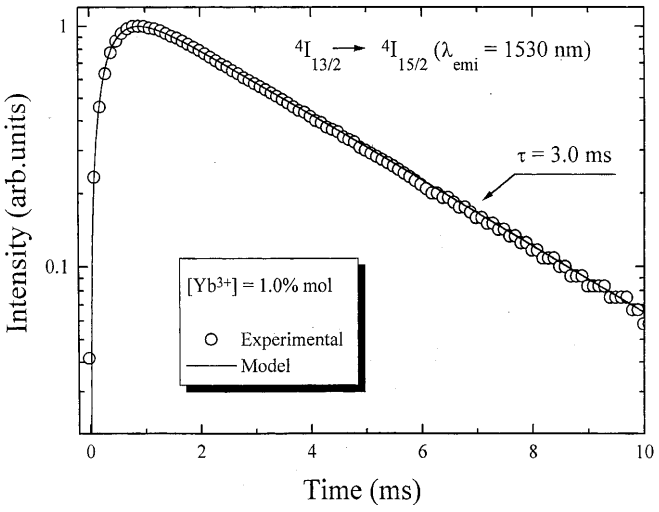

Fig. 2. Temporal evolution (in a logarithmic scale) of the luminescence of Er^{3+} ions ($^4I_{13/2} \rightarrow {}^4I_{15/2}$ transition), measured at 1.53 μm, after pulsed excitation of the Yb^{3+} ions at 920 nm, for a sample co-doped with 0.5 mol. % Er^{3+} and 1.0 mol. % Yb^{3+} (*open circles*). The *line* corresponds to the predictions from the integration of the rate (1)–(6)

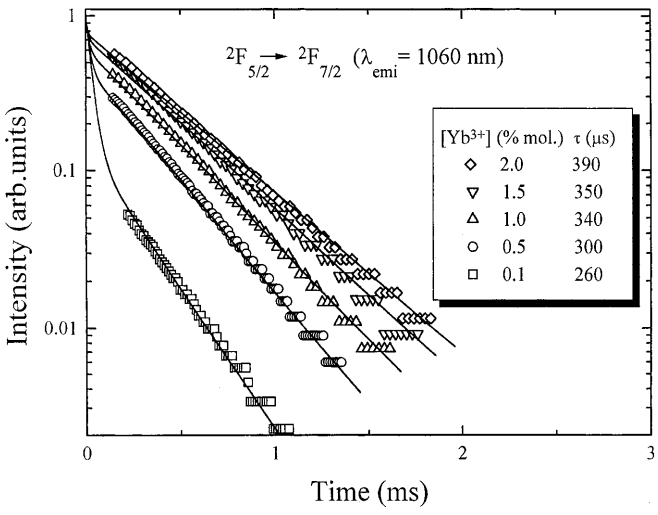

Fig. 3. Temporal evolution (in a logarithmic scale) of the luminescence of Yb^{3+} ions ($^2F_{5/2} \rightarrow {}^2F_{7/2}$ transition), measured at 1.06 μm for crystals with different Yb^{3+} concentration (*open symbols*). The *lines* correspond to the predictions from the integration of the rate (1)–(6)

transition) obtained in a sample co-doped with 1.0 mol. % of ytterbium (squares) pumped at 920 nm (Yb^{3+} absorption band) and that obtained in a sample singly doped with 0.5 mol. % of Er^{3+} (circles) pumped at 974 nm ($^4I_{15/2} \rightarrow {}^4I_{11/2}$ erbium absorption band). As can be observed, the lifetime of the $^4S_{3/2}$ manifold suffers a substantial increment from the 30 μs characteristic of Er^{3+} in lithium niobate [9] to a much slower decay in the Er^{3+}/Yb^{3+} system. This lengthening increases with the ytterbium content, and the lifetime varies from 100 μs (0.1 mol. % Yb^{3+}) to 210 μs in samples co-doped with 2.0 mol. % of ytterbium.

Another difference in the up-converted emission is the rise time of the luminescence. Whereas in co-doped samples this initial stage is clearly observed, lasting about 100 μs, it is absent in the Er^{3+} doped samples. This difference indicates that in the singly doped sample (excited to the Er^{3+} $^4I_{11/2}$ level), with a negligible rise time, the dominant process that populates the $^4S_{3/2}$ multiplet is the excited state absorption (ESA) [6, 7, 16], whereas in co-doped crystals, pumped through the Yb^{3+} absorption, and exhibiting a clear initial rise time the ESA mechanism is absent (or at least, it is not the dominant process). In this case, the principal mechanism that populates the $^4S_{3/2}$ level is the energy transfer via the cross-relaxation mechanism: $^2F_{5/2} \rightarrow {}^2F_{7/2}$ (Yb^{3+}) : $^4I_{11/2} \rightarrow {}^4F_{7/2}$ (Er^{3+}).

Using the estimated value for the up-conversion coefficient ($C_{26} = 4.8 \times 10^{-16}\,cm^3\,s^{-1}$), the rate equations give also the population of the $^4S_{3/2}$ level, and then the temporal dependence of the green luminescence. These results correspond to the continuous line in Fig. 4, which shows an excellent accordance with the experimental results, either in the lifetime of the decay as well as in the observed rise time; which supports the cross-relaxation model for the $^4S_{3/2}$ population.

The lifetime of the $^4S_{3/2}$ Er^{3+} multiplet, in the co-doped crystals, exhibits also a clear concentration dependence, in a similar way to the Yb^{3+} luminescence described in the preceding section. This is a direct consequence of the fact, already mentioned above, that the dominant process which populates the $^4S_{3/2}$ level in co-doped samples is the cross relaxation from the $^2F_{5/2}$ Yb^{3+} level ($^2F_{5/2} \rightarrow {}^2F_{7/2}$ (Yb^{3+}): $^4I_{11/2} \rightarrow {}^4F_{7/2}$ (Er^{3+})), and therefore the 550-nm emission lifetime follows a concentration dependence parallel to that of the 1060-nm emission.

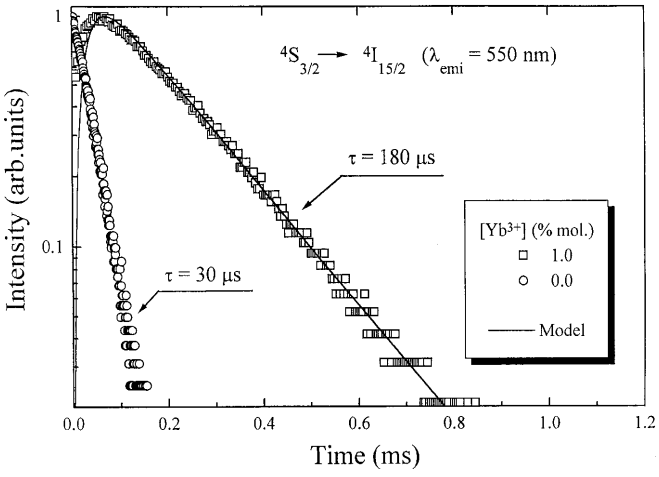

Fig. 4. Temporal evolution of the green up-conversion luminescence of Er^{3+} ($^4S_{3/2} \rightarrow {}^4I_{15/2}$ transition) in a sample singly doped with Er^{3+} (*circles*) and in a sample co-doped with Er^{3+} and Yb^{3+} (*squares*). The *line* corresponds to the prediction of the rate (1)–(6)

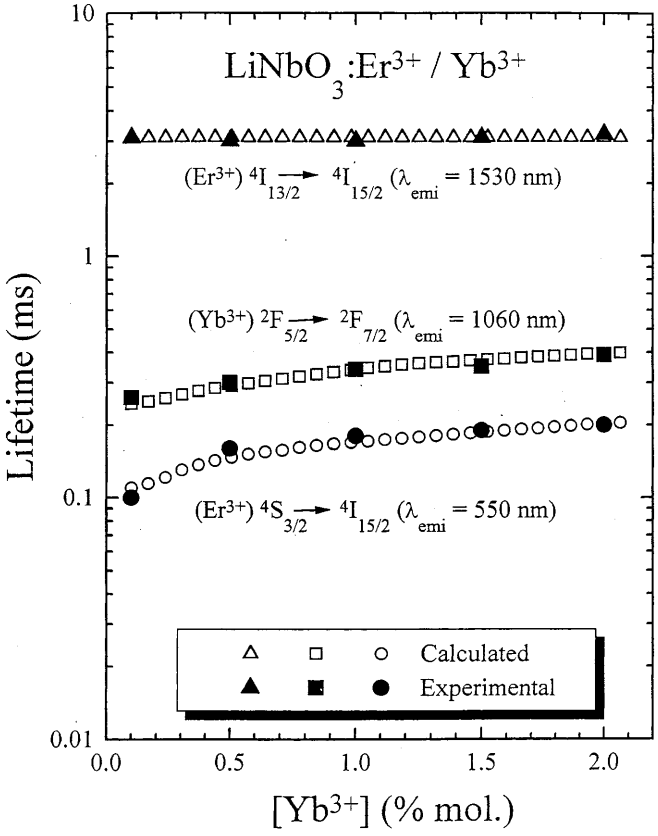

Fig. 5. Experimental (*full symbols*) and calculated (*open symbols*) lifetimes for the different luminescent emissions of $LiNbO_3$:Er^{3+}/Yb^{3+} as function of Yb^{3+} concentration

The concentration dependence of the different emissions lifetime is summarised in Fig. 5, where the experimental values (full symbols) are compared with the predictions from the rate-equation model calculated (open symbols) for several Yb^{3+} concentrations and a fixed (0.5 mol. %) erbium concentration. The results are coincident within 5%.

3 Conclusion

The dynamic behaviour of the principal luminescent emissions observed in $LiNbO_3$ co-doped with Er^{3+} and Yb^{3+}, at different doping levels, has been obtained after pulsed excitation. The temporal dependence of the IR transitions is explained by using the rate-equation formalism and cross-relaxation model for the energy transfer, using the transfer parameters previously obtained under cw conditions ($C_{25} = 2.4 \times 10^{-16}\,cm^3\,s^{-1}$ and $C_{52} = 1.8 \times 10^{-16}\,cm^3\,s^{-1}$).

The visible luminescence is also explained using the same formalism and another cross-relaxation mechanism to populate the upper Er^{3+} levels (up-conversion). The up-conversion transfer coefficient is given by $C_{26} = 4.8 \times 10^{-16}\,cm^3\,s^{-1}$.

The sensitisation of the $LiNbO_3$:Er^{3+} system with Yb^{3+} ions does not modify the lifetime of the $^4I_{13/2}$ erbium level (1.5-μm emission), whereas it induces a marked,

concentration-dependent change in the lifetime of the $^2F_{5/2}$ (Yb^{3+}) and $^4S_{3/2}$ (Er^{3+}) multiplets (1060-nm and 550-nm emissions, respectively), which is also correctly described with the model and spectroscopic parameters proposed.

Acknowledgements. This work is partially supported by CICYT (PB97-0019) and Comunidad de Madrid (07T/0026/1998).

References

1. E. Cantelar, J.A. Muñoz, J.A. Sanz-García, F. Cussó: J. Phys.: Condens. Matter **10**, 8893 (1998)
2. R. Brinkman, W. Sohler, H. Suche: Electron. Lett. **27**, 415 (1991)
3. K. Schäfer, I. Baumann, W. Sohler, H. Suche, S. Westenhöfer: IEEE J. Quantum Electron. **QE-33**, 1636 (1997)
4. D. Barbier, M. Rattay, F. Saint André, G. Clauss, M. Trouillon, A. Kevorkian, J.M.P. Delavaux, E. Murphy: IEEE Photon. Tech. Lett. **9**, 315 (1997)
5. J.A. Muñoz, B. Herreros, G. Lifante, F. Cussó: Phys. Status Solidi A **168**, 525 (1998)
6. C. Huang, L. McCaughan: IEEE Photon. Tech. Lett. **9**, 599 (1997)
7. P.E.A. Möbert, E. Heumann, G. Huber: Opt. Lett. **22**, 1412 (1997)
8. J.A. Muñoz, R.E. Di Paolo, R. Duchowicz, J.O. Tocho, F. Cussó: Solid State Commun. **107**, 487 (1998)
9. L. Núñez, G. Lifante, F. Cussó: Appl. Phys. B **62**, 485 (1996)
10. J. Amin, B. Dussardier, T. Schweizer, M. Hempstead: J. Lumin. **69**, 17 (1996)
11. L.F. Johnson, H.J. Guggenheim, T.C. Rich, F.W. Ostermayer: J. Appl. Phys. **43**, 1125 (1972)
12. B. Zandi, L.D. Merkle, J.A. Hutchinson, H.R. Verdun, B.H.T. Chai: J. Phys. IV C4-587 (1994)
13. B. Simondi-Teisseire, B. Viana, D. Vivien, A.M. Lejus: Opt. Mater. **6**, 267 (1996)
14. Chr. Wyss, W. Lüthy, H.P. Weber, P. Rogin, J. Hulliger: Opt. Commun. **144**, 31 (1997)
15. I.R. Martin, V.D. Rodriguez, V. Lavin, U.R. Rodriguez-Mendoza: J. Lumin. **72-74**, 954 (1997)
16. J. Koetke, G. Huber: Appl. Phys. B **61**, 151 (1995)